# The effect of doping $CaBr_2$ on the $CsPbBr_3$ film for photovoltaic application

FEI ZHAO[1,*], YIXIN GUO[2,*], PEIZHI YANG[3], JUNHAO CHU[4]
[1]*School of Photoelectric Engineering, Changzhou Institute of Technology, Changzhou, Jiangsu, 213002, China*
[2]*Department of Physics, Shanghai Normal University, Shanghai 200233, China*
[3]*Key Laboratory of Advanced Technique & Preparation for Renewable Energy Materials, Ministry of Education, Yunnan Normal University, Kunming 650500, China*
[4]*Shanghai Institute of Technical Physics, Chinese Academy of Sciences, Shanghai 200083, China*

All-inorganic perovskite $CsPbBr_3$ has gained widespread attention for photovoltaic application due to its preeminent stability. However, the conversion efficiency of $CsPbBr_3$ solar cell is relatively low. Herein, a novel doping strategy has been employed in $CsPbBr_3$ solar cell, which generates multiple benefits to enhance the cell performance. After doping $CaBr_2$, carbon-based $CsPbBr_3$ solar cell achieves a higher efficiency of 2.48%. The mechanism behind the efficiency improvement is that $CaBr_2$-doped $CsPbBr_3$ films have higher crystallinity, smaller optical band gap, and lower carrier recombination probability. This work opens up a simple and efficient method for enhancing the photovoltaic performance of all-inorganic perovskite solar cell.

(Received August 29, 2024; accepted June 4, 2025)

*Keywords*: $CsPbBr_3$, Doping $CaBr_2$, Optical band gap, Perovskite solar cell

## 1. Introduction

Organic-inorganic halide perovskite (OIHP) has become a highly promising material in photovoltaic field due to its adjustable band gap and long carrier diffusion length [1]. At present, the efficiency of OIHP solar cell has increased from 3.8% to 26.1% [2-4]. The high efficiency of OIHP cells makes them the most promising alternative to silicon solar cells. Nevertheless, the instability of OIHP cell stemming from the organic components in OIHP seriously hinders its development of commercialization [5-7]. Thus, employing inorganic Cs ions instead of organic components to enhance the stability of devices has been considered as a good strategy to boost the commercial development. Especially, all-inorganic $CsPbI_xBr_{3-x}$ ($0 \le x \le 3$) cell device has been widely studied owing to its distinctive optoelectronic properties and surprising stability [8-10]. Among these devices, the all bromine-based $CsPbBr_3$ cell has preeminent durability under continuous moisture attack [11-13].

High-crystallinity $CsPbBr_3$ layers and corresponding high-quality devices can be prepared using specific techniques. Using vacuum deposition technology [14] and solution spin coating technology [15] can prepare high-quality $CsPbBr_3$ layers and corresponding devices. However, vacuum deposition technology requires high vacuum conditions to prepare high-quality samples, which greatly increases the preparation cost. On the contrary, solution spin coating technology can prepare high-quality $CsPbBr_3$ in air. Therefore, solution spin coating technology is more suitable for preparing $CsPbBr_3$. In addition, doping strategies can effectively improve the quality of $CsPbBr_3$ layers and the corresponding device efficiency. According to literature report [16], doping Mn, Ni, Cu and Zn elements can enhance the efficiency of $CsPbBr_3$ devices with carrier transport layers. Moreover, this leads to complex device fabrication processes and increased fabrication costs because these $CsPbBr_3$ cells contain carrier transport layers. Therefore, it is necessary to prepare $CsPbBr_3$ cell with simple structure. However, there are relatively few reports on Ca-doped $CsPbBr_3$ cells without carrier transport layers.

In this work, we prepare $CsPbBr_3$ cells without carrier transport layers. Meanwhile, $CaBr_2$ is further incorporated into $CsPbBr_3$ devices. After the introduction of $CaBr_2$, the conversion efficiency of the $CsPbBr_3$ device can be effectively enhanced (2.48%). This phenomenon is due to the better quality of $CsPbBr_3$ layers.

## 2. Experimental

### 2.1. Preparation of solar cells

The FTO substrates with size of 2×2 $cm^2$ were

cleaned with deionized water, acetone, isopropanol and ethanol, successively. The $CsPbBr_3$ perovskite layer was prepared exploiting a multistep solution-processed method. 367 mg $PbBr_2$ was dissolved into 1 ml DMF and stirred at 90 ℃ for 8 h to acquire a limpid solution. Before the preparation of $PbBr_2$ layer, the FTO substrate was preheated at 90 ℃. Subsequently, the limpid $PbBr_2$ solution was spin-coated at 2000rpm for 30s. Afterwards, the $PbBr_2$ layer was instantly heated at 90 ℃ for 30 min. After that, 15 mg CsBr in 1ml methanol solution was deposited on $PbBr_2$ layer at 2000rpm for 30 s. Then, the CsBr layer was annealed at 250 ℃ for 5min. This procedure was duplicated for four times to acquire $CsPbBr_3$ layer. To manufacture whole carbon-based $CsPbBr_3$ cell, a carbon electrode with active area of 0.09 $cm^2$ was prepared on $CsPbBr_3$ layer. Eventually, the carbon electrode was heated at 120 ℃ for 15min. For $CaBr_2$-doped cell, the $CaBr_2$ was directly added to the limpid $PbBr_2$ solution. The other steps followed the above steps. All manufacturing processes were carried out in an air atmosphere.

### 2.2. Characterizations

The chemical composition of sample was tested through XPS. The surface morphology of sample was obtained by SEM. The absorption spectra for different samples were recorded by employing a UV-vis spectrophotometer. The steady-state PL spectra for various samples were gained from photoluminescence spectrometer. The TRPL spectra for different samples were also conducted. The J-V curves of solar cells were gained under standard AM 1.5G.

## 3. Results and discussions

### 3.1. Analysis of $CsPbBr_3$ perovskite film

The SEM images of the undoped and $CaBr_2$-doped $CsPbBr_3$ layers are given in Fig. 1. The undoped $CsPbBr_3$ layer has poor uniformity and its average grain size is small (560 nm). This leads to the presence of a large number of grain boundaries in undoped $CsPbBr_3$ layer. For $CaBr_2$-doped $CsPbBr_3$ layer, it possesses a good uniformity. The average grain size of $CaBr_2$-doped $CsPbBr_3$ layer is boosted to 697 nm, which results in reduced grain boundaries. The improved grain sizes may enhance the crystallinity of $CsPbBr_3$ layer, and reduce its number of grain boundaries. This is beneficial for improving charge transfer capability and suppressing carrier recombination rate, which helps to increase short-circuit current density ($J_{sc}$), open-circuit voltage ($V_{oc}$) and fill factor (FF) [17].

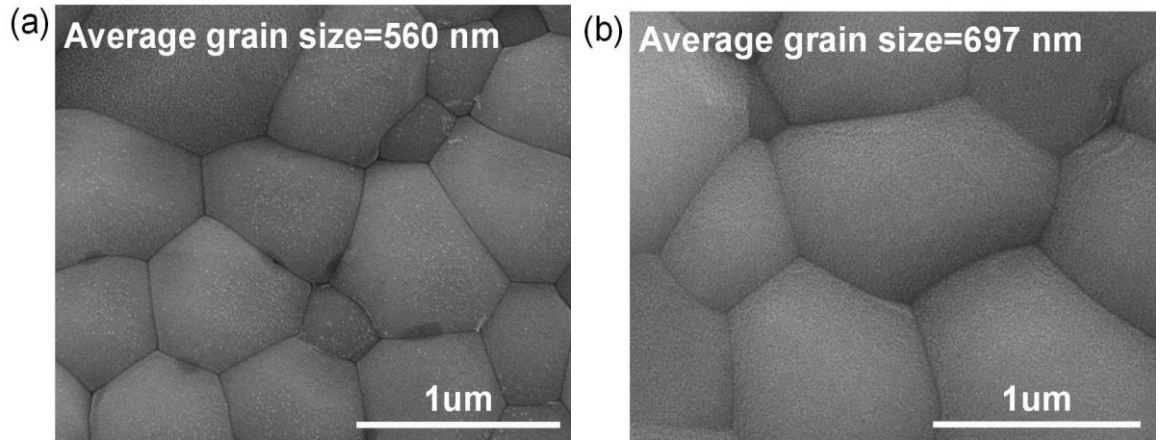


*Fig. 1. Top-view SEM images of $CsPbBr_3$ films (a) without $CaBr_2$ and (b) with $CaBr_2$*

The XPS spectra are gained to reveal the chemical states of the undoped and $CaBr_2$-doped $CsPbBr_3$ perovskites, as drawn in Fig. 2a and 2b. It is worth noting that the peak position of Pb element shifts towards higher binding energy after doping $CaBr_2$. The peak positions corresponding to Pb $4f_{3/2}$ and Pb $4f_{5/2}$ shift from 142.85 eV and 137.99 eV to a higher binding energy of 143.10 eV and 138.21eV after doping $CaBr_2$.

The peak shift behaviors originate from the insertion of Ca ions into the $CsPbBr_3$ lattice [18]. The two peaks at 351.09eV and 347.39 eV corresponding to Ca 2p is found in the $CaBr_2$-doped $CsPbBr_3$ layer. This confirms the presence of Ca element in the $CsPbBr_3$ layer. The relatively weak intensity of the two peaks may be caused by low doping level.

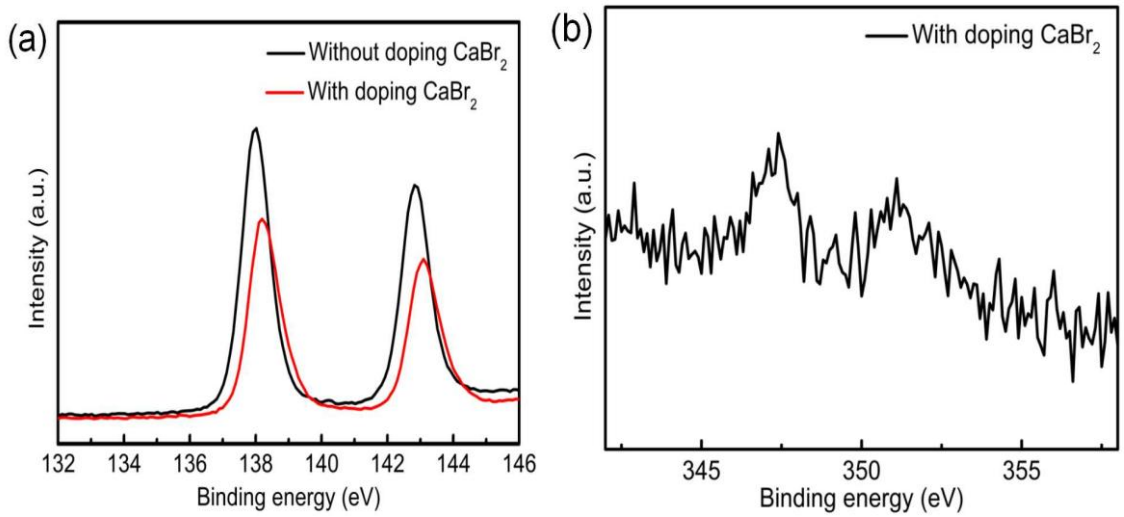


*Fig. 2. (a) XPS spectra (Pb 4f) of $CsPbBr_3$ films without and with $CaBr_2$. (b) XPS spectra (Ca 2p) of the undoped and $CaBr_2$-doped $CsPbBr_3$ films (colour online)*

Fig. 3a indicates the absorption spectra of the undoped and $CaBr_2$-doped $CsPbBr_3$ layers. The absorption intensity of $CaBr_2$-doped $CsPbBr_3$ layer is higher compared with undoped $CsPbBr_3$ layer, which is attributed to the crystallinity improvement of $CaBr_2$-doped $CsPbBr_3$ layer. In addition, the increase of the absorption peak intensity is beneficial for absorbing more sunlight. Fig. 3b shows the optical band gaps of the undoped and $CaBr_2$-doped $CsPbBr_3$ films. For $CsPbBr_3$ layer without doping $CaBr_2$, it optical band gap is 2.34 eV. The optical band gap of $CaBr_2$-doped $CsPbBr_3$ layer is decreased to 2.33 eV. The reduction of the band gap for the $CsPbBr_3$ layer originates from the incorporation of Ca ions into the $CsPbBr_3$ layer. Meanwhile, the the band gap reduction also can absorb more sunlight, which is consistent with the previous analysis results.

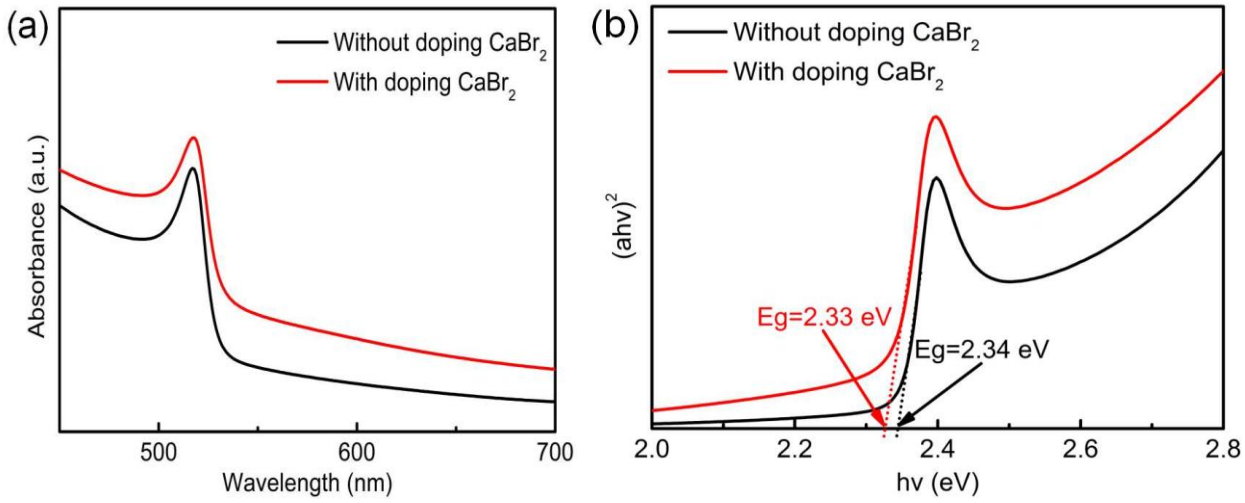


*Fig. 3. (a) Absorption spectra and (b) optical band gaps of the undoped and $CaBr_2$-doped $CsPbBr_3$ films (colour online)*

Fig. 4a indicates the steady-state PL spectra of the undoped and $CaBr_2$-doped $CsPbBr_3$ layers. The undoped $CsPbBr_3$ layer presents a weaker PL emission peak, suggesting that more defect sites exist in the undoped $CsPbBr_3$ layer. The stronger PL intensity for the $CsPbBr_3$ layer with doping $CaBr_2$ shows the existing of less defects. The existence of defects is due to the presence of grain boundaries in the film. As the number of grain boundaries decreases, the number of defect sites also reduces. The TRPL spectra of these $CsPbBr_3$ layers are also presented in Fig. 4b. The PL lifetime can be well fitted through a biexponential equation (1):

$$f(t)=A_1\exp(-t/\tau_1)+A_2\exp(-t/\tau_2)+B \quad (1)$$

Here, $\tau_1$ and $\tau_2$ stand for the slow and fast decay time

constants, separately. $A_1$ and $A_2$ stand for the corresponding fractional amplitudes of $\tau_1$ and $\tau_2$. In addition, B stands for a constant. The average carrier lifetime $\tau_{ave}$ is obtained through equation (2):

$$\tau_{ave}=\sum A_i\tau_i/\sum A_i \quad (2)$$

For the $CsPbBr_3$ layer without doping $CaBr_2$, its average carrier lifetime is 17.69 ns. However, The average carrier lifetime of the $CaBr_2$-doped $CsPbBr_3$ layer increases to 27.50 ns. This is because the $CaBr_2$-doped $CsPbBr_3$ layer has obtained higher crystallinity. The higher $\tau_{ave}$ value of the $CaBr_2$-doped $CsPbBr_3$ layer reveals the carrier recombination rate in the bulk perovskite is effectively restrained [10].

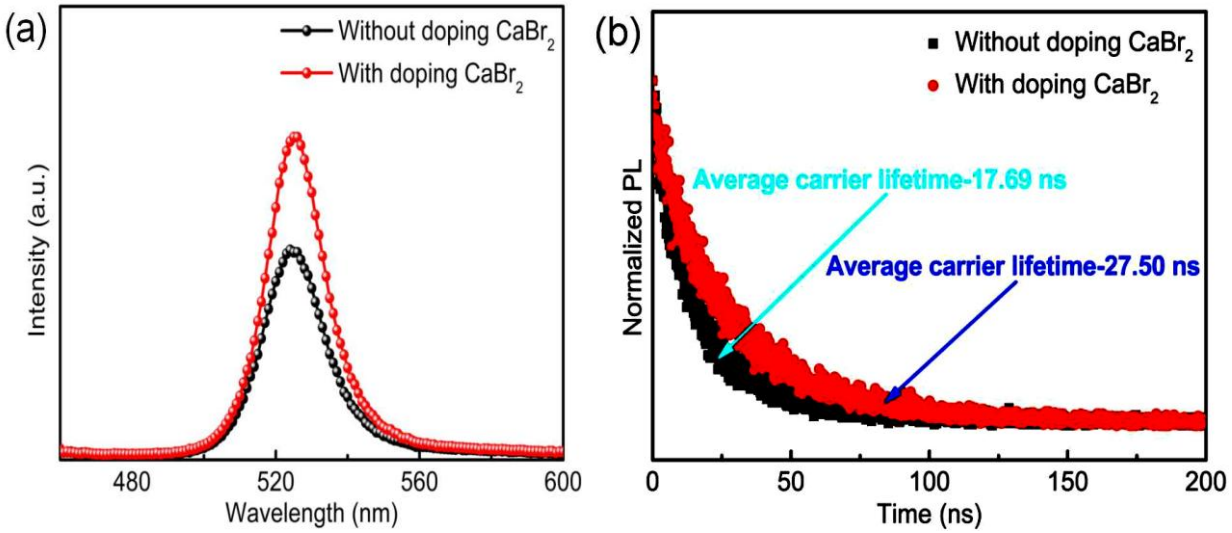


*Fig. 4. (a) PL spectra and (b) TRPL spectra of the undoped and $CaBr_2$-doped $CsPbBr_3$ films (colour online)*

### 3.2. Analysis of $CsPbBr_3$ solar cell

Fig. 5 shows the cross-sectional SEM image of the complete cell. The entire cell device is composed of FTO, $CsPbBr_3$ and carbon electrode. Each layer in the cell is in close contact, indicating that our device has high quality.

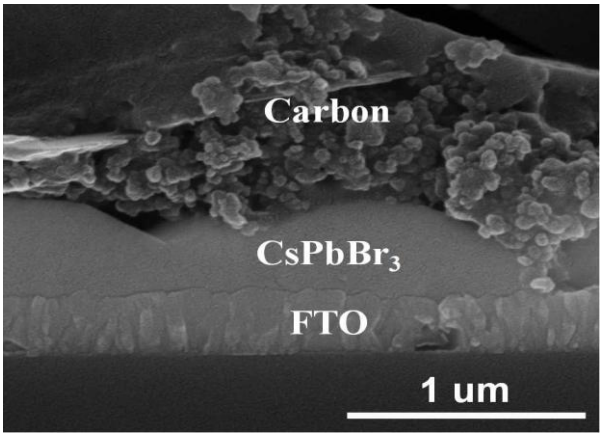


*Fig. 5. Cross-sectional SEM image of the $CsPbBr_3$ device*

The J-V characteristics and the corresponding photovoltaic parameters of the best-performing cells prepared through the undoped and $CaBr_2$-doped $CsPbBr_3$ layers are shown in Fig. 6. The best device based on the undoped $CsPbBr_3$ layer exhibits a low efficiency of only 1.73%, with a $V_{oc}$ of 1.100 V, a $J_{sc}$ of 3.51 mA/cm$^2$, and a FF of 44.75%. However, all the photovoltaic parameters for the devices containing $CaBr_2$-doped $CsPbBr_3$ layers are dramatically improved ($V_{oc}$=1.179 V, $J_{sc}$=4.03 mA/cm$^2$, FF=52.23%), resulting in a higher efficiency of 2.48%. The reason for the efficiency improvement is that the $CsPbBr_3$ layer with doping $CaBr_2$ has higher crystallinity, lower optical bandgap and less carrier recombination [19].

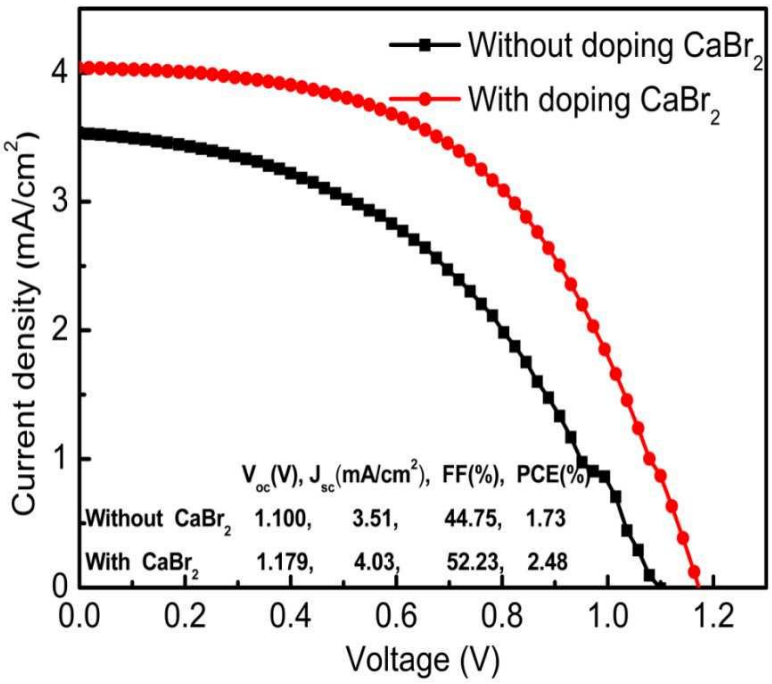


*Fig. 6. J-V curves of the undoped and $CaBr_2$-doped $CsPbBr_3$ films (colour online)*

## 4. Conclusions

This study establishes a simple doping strategy to achieve the incorporation of $CaBr_2$ in $CsPbBr_3$ cells. Its crystallinity has been significantly improved by introducing $CaBr_2$ into $CsPbBr_3$ films. Meanwhile, the optical band gap of $CaBr_2$-doped $CsPbBr_3$ film is smaller compared with undoped $CsPbBr_3$ film. In addition, $CaBr_2$-doped $CsPbBr_3$ film also possesses a lower carrier recombination probability. A best efficiency of 2.48% for low-cost $CaBr_2$-doped $CsPbBr_3$ cell without utilizing electron-hole transport layers can be accomplished. This work can be well extended to other various inorganic cells, which paves the way for the preparation of high-performance and stable inorganic optoelectronic devices.

### Acknowledgements

This work was financed by the National Natural Science Foundation of China (Grant No. 12304043), the Key Applied Basic Research Program of Yunnan Province (Grant No. 202201AS070023) and Yunnan Revitalization Talent Support Program, the Spring City Plan: High-level Talent Promotion and Training Project of Kunming (Grant No. 2022SCP005).

## References

[1] R. Lin, K. Xiao, Z. Qin, Q. Han, C. Zhang, M. Wei, M. I. Saidaminov, Y. Gao, J. Xu, M. Xiao, A. Li, J. Zhu, E. H. Sargent, H. Tan, Nat. Energy **4**, 864 (2019).
[2] X. Jiang, C. Geng, X. Yu, J. Pan, H. Zheng, C. Liang, B. Li, F. Long, L. Han, Y. Cheng, Y. Peng, ACS Appl. Mater. Interfaces **16**, 19039 (2024).
[3] B. Yuan, Y. Zhou, T. Liu, C. Li, B. Cao, ACS Sustainable Chem. Eng. **11**, 718 (2023).
[4] J. Chen, Z. Wu, S. Chen, W. Zhao, Y. Zhang, W. Ye, R. Yang, L. Gong, Z. Peng, J. Chen, Mat. Sci. Semicon. Proc. **174**, 108186 (2024).
[5] S. Yun, Y. Qin, A. R. Uhl, N. Vlachopoulos, M. Yin, D. Li, X. Han, A. Hagfeldt, Energy Environ. Sci. **11**, 476 (2018).
[6] W. Shao, J. Sheng, Y. Fu, J. He, Z. Deng, R. Cen, W. Wu, Energy Environ. Sci. **18**, 3211 (2025).
[7] Q. A. Akkerman, G. Raino, M. V. Kovalenko, L. Manna, Nat. Mater. **17**, 394 (2018).
[8] D. Bai, J. Zhang, Z. Jin, H. Bian, K. Wang, H. Wang, L. Liang, Q. Wang, S. Liu, ACS Energy Lett. **3**, 970 (2018).
[9] Y. Zheng, X. Yang, R. Su, P. Wu, Q. Gong, R. Zhu, Adv. Funct. Mater. **30**, 2000457 (2020).
[10] X. Liu, X. Tan, Z. Liu, H. Ye, B. Sun, T. Shi, Z. Tang, G. Liao, Nano Energy **56**, 184 (2019).
[11] J. Duan, Y. Zhao, B. He, Q. Tang, Angew. Chem. Int. Ed. **57**, 3787 (2018).
[12] J. Liang, C. Wang, Y. Wang, Z. Xu, Z. Lu, Y. Ma, H. Zhu, Y. Hu, C. Xiao, X. Yi, G. Zhu, H. Lv, L. Ma, T. Chen, Z. Tie, Z. Jin, J. Liu, J. Am. Chem.

Soc. **138**, 15829 (2016).
[13] J. Zhu, M. Tang, B. He, K. Shen, W. Zhang, X. Sun, M. Sun, H. Chen, Y. Duan, Q. Tang, Chem. Eng. J. **404**, 126548 (2021).
[14] J. Lei, F. Gao, H. Wang, J. Li, J. Jiang, X. Wu, R. Gao, Z. Yang, S.F. Liu, Sol. Energy Mater. Sol. Cells **187**, 1 (2018).
[15] F. Zhao, Y. Guo, J. Tao, Z. Li, J. Jiang, J. Chu, Appl. Optics **59**, 5481 (2020).
[16] M. Tang, B. He, D. Dou, Y. Liu, J. Duan, Y. Zhao, H. Chen, Q. Tang, Chem. Eng. J. **375**, 121930 (2019).
[17] X. Liu, Z. Liu, X. Tan, H. Ye, B. Sun, S. Xi, T. Shi, Z. Tang, G. Liao, J. Power Sources **439**, 227092 (2019).
[19] J. K. Nam, S. U. Chai, W. Cha, Y. J. Choi, W. Kim, M. S. Jung, J. Kwon, D. Kim, J. H. Park, Nano Lett. **17**, 2028 (2017).
[20] X. Wan, Z. Yu, W. Tian, F. Huang, S. Jin, X. Yang, Y. Cheng, A. Hagfeldt, L. Sun, J. Energy Chem. **46**, 8 (2020).

*Corresponding author: fzhaobs@126.com;
yxguo@shnu.edu.cn